



OPEN ACCESS

EDITED BY

Xiaohu Yang,
Xi'an Jiaotong University, China

REVIEWED BY

Zhexi Wen,
Central South University, China
Koichi Ichimiya,
University of Yamanashi, Japan
Yuetao Shi,
Shandong University, China

*CORRESPONDENCE

Jianyong Wang,
✉ wangjiany5@mail.sysu.edu.cn

RECEIVED 29 June 2023

ACCEPTED 01 August 2023

PUBLISHED 14 August 2023

CITATION

Yang J, Xie X, Tang G and Wang J (2023),
Computational investigation on turbulent
heat transfer of supercritical CO₂ in the
half-roughen horizontal pipe.
Front. Energy Res. 11:1249849.
doi: 10.3389/fenrg.2023.1249849

COPYRIGHT

© 2023 Yang, Xie, Tang and Wang. This is
an open-access article distributed under
the terms of the [Creative Commons
Attribution License \(CC BY\)](#). The use,
distribution or reproduction in other
forums is permitted, provided the original
author(s) and the copyright owner(s) are
credited and that the original publication
in this journal is cited, in accordance with
accepted academic practice. No use,
distribution or reproduction is permitted
which does not comply with these terms.

Computational investigation on turbulent heat transfer of supercritical CO₂ in the half-roughen horizontal pipe

Jun Yang, Xiongzhou Xie, Guowei Tang and Jianyong Wang*

School of Aeronautics and Astronautics, Sun Yat-sen University, Guangzhou, Guangdong, China

To address the heat transfer degradation that occurs in the top section of horizontal pipes when sCO₂ fluid flows are heated, the upper half wall with higher temperatures is particularly roughened using uniform sand-grain roughness. The SST $k-\omega$ model is validated and used to simulate the horizontal sCO₂ heat transfer involving a variety of operating parameters and roughness heights. Results indicate that the half-roughen scheme is effective in significantly reducing higher temperatures of the entire upper wall and improving heat transfer homogeneity. The roughness height plays a crucial role, and an optimal value exists, which is largely influenced by the buoyancy strength and its local variations of horizontal sCO₂ flows under different conditions.

KEYWORDS

supercritical CO₂, horizontal, half-roughen, roughness height, buoyancy

1 Introduction

Supercritical CO₂ (sCO₂) has gained widespread recognition as an ideal working fluid for various energy and power cycles, owing to its several distinct advantages. These include favorable properties that enable higher cycle efficiency (Mendez Cruz and Rochau, 2018), reduced compression work and cycle size due to its high density, and a more accessible critical pressure ($P_{cr} = 7.38$ MPa) compared to water, where the supercritical state is achieved at a much higher point of $P_{cr} = 22.1$ MPa. Consequently, the use of sCO₂ as a heat transfer carrier has garnered significant attention for promising renewable energy sources, such as concentrating solar thermal (Yang et al., 2021), nuclear (Wu et al., 2020), and geothermal (Yalcinkaya and BIYIKOĞLU, 2012) energy.

In the proximity of the critical and pseudocritical points, sCO₂ thermophysical properties undergo significant changes, leading to peculiar heat transfer behaviors. One of these behaviors is the heat transfer deterioration and heterogeneity that occur in horizontal sCO₂ fluid flows. As demonstrated in the work of Kumar and Basu (2021) and Theologou et al. (2022), temperatures of the top wall are much higher, and the heat transfer is severely degraded. This impairment near the top not only negatively affects the overall heat transfer performance but also causes greater wall thermal stress, which poses a threat to the safety of heat exchange equipment. To relieve supercritical heat transfer deterioration in the top and improve uniformity over the periphery, fins (Han et al., 2022),

Abbreviations: sCO₂, supercritical carbon dioxide; DNS, direct numerical simulation; and CFD, computational fluid dynamics.

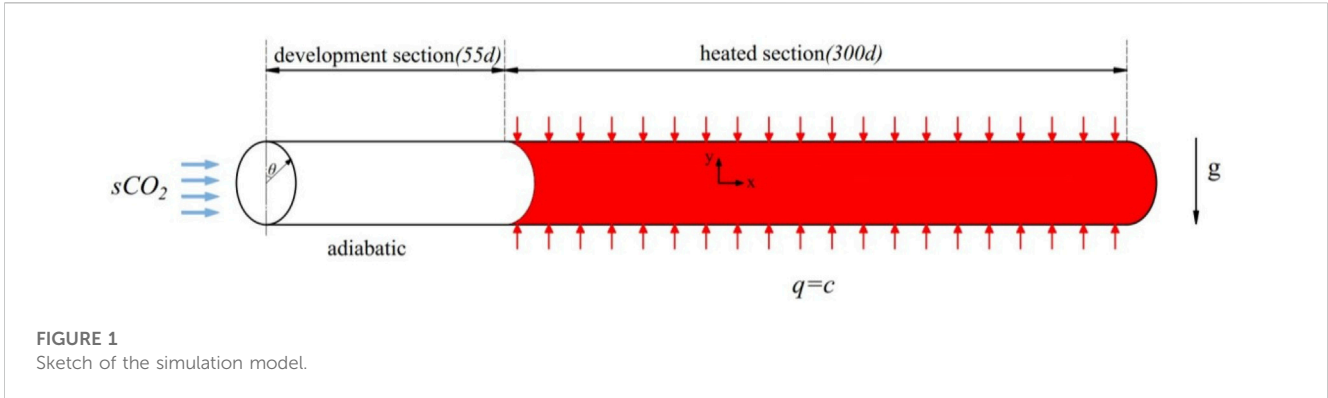


TABLE 1 Cases to be validated from the measurements by [Chen et al. \(2022\)](#).

Test code	Mass flux G (kg/m ² · s)	Heat flux q (kW/m ²)	Pressure P (MPa)	Roughness height Δ (μm)
T1	500	50	9	1.5
T2	500	50	9	40
T3	400	50	9	40
T4	500	60	8	40
T5	400	40	8	30

internal ribs ([Mao et al., 2022](#)), and metal foams ([Liu et al., 2015](#)) have been added and studied. These technologies have been shown to notably improve horizontal sCO₂ heat transfer; however, they also have non-negligible drawbacks, such as high manufacturing and maintenance costs and significant extra friction loss.

The use of wall roughness, particularly sand-grain roughness, has been explored to enhance turbulent heat transfer of channel flows. With the aid of direct numerical simulation (DNS), [Forooghi et al. \(2018\)](#) systematically studied the influence of sand-grain roughness on the convection heat transfer of turbulent channel flows and observed the augmentation of heat transfer. [Latini et al. \(2022\)](#) numerically modeled the increased heat transfer of coolant flow for liquid rocket engines with high surface roughness. With the help of additive manufacturing, [Stimpson et al. \(2016\)](#) measured heat transfer with wall roughness and found much higher Nusselt numbers than in smooth channels. Although significant heat transfer enhancements have been demonstrated in the literature, wall roughness is barely investigated in supercritical heat transfer. [Zhang et al. \(2020\)](#) comprehensively reviewed the enhancing technologies used for turbulent sCO₂ heat transfer and suggested that wall roughness is a potential approach to effectively mitigate the deterioration. Most recently, [Chen et al. \(2022\)](#) first introduced sand-grain wall roughness to improve sCO₂ heat transfer in a vertical tube, demonstrating remarkable mitigation of heat transfer impairment as evidenced by the drops in measured wall temperatures.

This study utilizes the uniform sand-grain wall roughness as a means to alleviate heat transfer degradation and improve homogeneity over the circumference of turbulent sCO₂ flowing through horizontal tubes. The half-roughen scheme was used, which focuses specifically on the upper half surface where

deterioration occurs. Computational fluid dynamics (CFD) simulations are conducted employing the SST $k-\omega$ model, which is thoroughly validated against experiments. Then, with the help of this reliable CFD tool, the influences of roughness height and typical operating parameters are investigated, and the variations and mechanisms are analyzed in detail. Moreover, the important selection criteria for roughness heights under different conditions has been identified.

2 Numerical approach

2.1 Governing equations

The horizontal sCO₂ flows are solved by the steady Navier–Stokes equations, which are formulated as follows based upon the Cartesian coordinates.

Continuity:

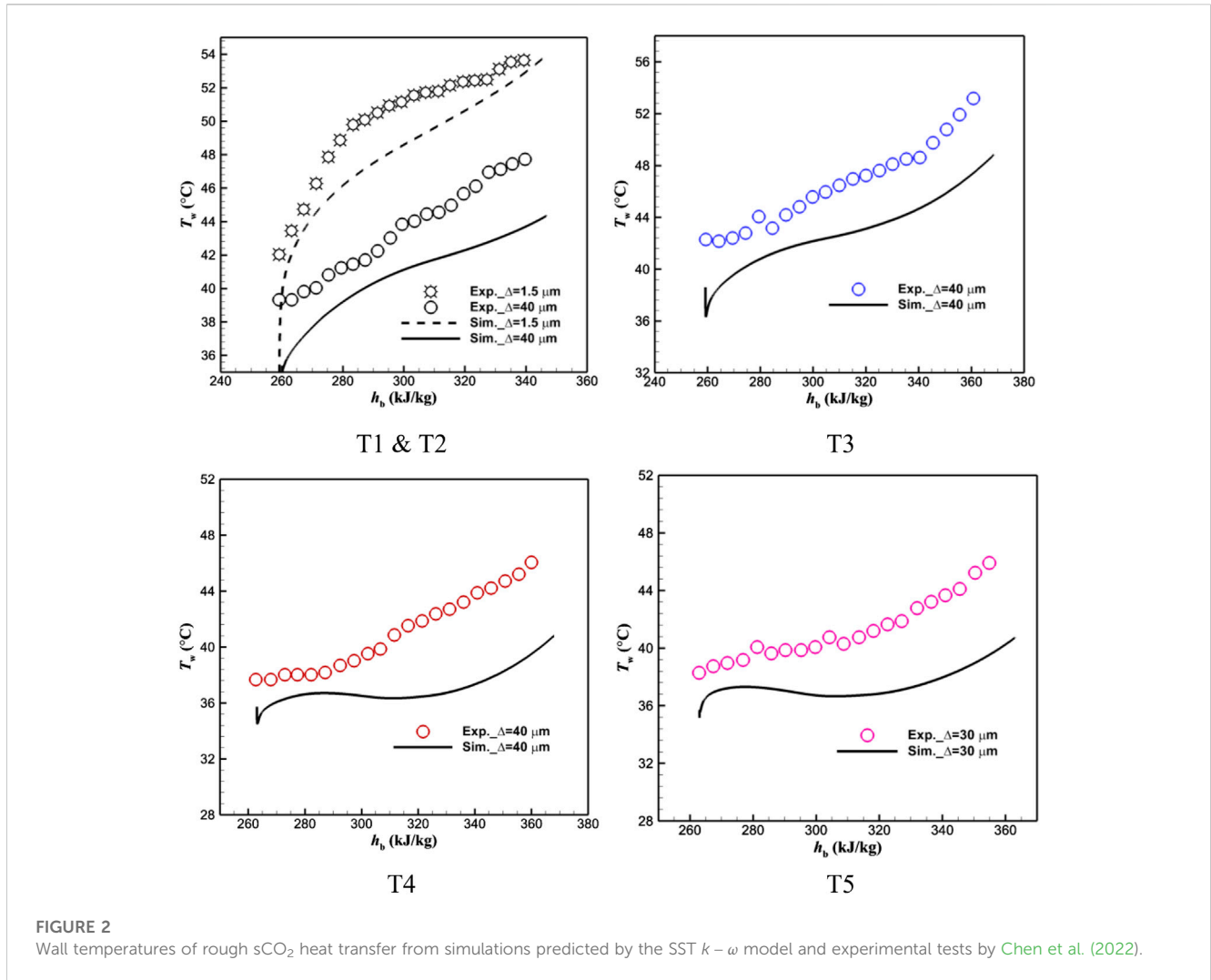
$$\frac{\partial}{\partial x_i} (\rho u_i) = 0. \tag{1}$$

Momentum:

$$\frac{\partial}{\partial x_j} (\rho u_i u_j) = -\frac{\partial P}{\partial x_i} + \rho g_i + \frac{\partial}{\partial x_j} \left[\mu \left(\frac{\partial u_i}{\partial x_j} + \frac{\partial u_j}{\partial x_i} \right) \right] + \frac{\partial}{\partial x_j} (-\rho \overline{u_i u_j}). \tag{2}$$

Energy:

$$\frac{\partial}{\partial x_i} (\rho u_i H) = \frac{\partial}{\partial x_i} \left(\lambda \frac{\partial T}{\partial x_i} - \rho \overline{u_i h} \right) + \mu \varphi - \frac{\partial u_i}{\partial x_j} (\rho \overline{u_i u_j}), \tag{3}$$



where λ represents the fluid thermal conductivity and φ represents the energy dissipation term.

$$\varphi = \left(\frac{\partial u_i}{\partial x_j} + \frac{\partial u_j}{\partial x_i} \right) \frac{\partial u_i}{\partial x_j} \quad (4)$$

Due to the good capability of dealing with both the boundary and core flows, the SST *k* – *ω* turbulence model performs well in predicting supercritical fluid flow and heat transfer ([Han et al., 2022](#); [Chen et al., 2023](#)), which is, thus, chosen in this study. The equations for the turbulence term of *k* and *ω* are as follows:

$$\frac{\partial}{\partial x_i} (\rho k u_i) = \frac{\partial}{\partial x_j} \left(\Gamma_k \frac{\partial k}{\partial x_j} \right) + \overline{G_k} - Y_k + S_k, \quad (5)$$

$$\frac{\partial}{\partial x_i} (\rho \omega u_i) = \frac{\partial}{\partial x_j} \left(\Gamma_\omega \frac{\partial \omega}{\partial x_j} \right) + G_\omega - Y_\omega + D_\omega + S_\omega. \quad (6)$$

More details on the various terms and model constants can be found in the work of [Menter \(1994\)](#).

2.2 Physical model and simulation methods

[Figure 1](#) displays the horizontal round tube ($d = 22.14 \text{ mm}$) used in this study, where the full three-dimensional model is built and the *x*- (axial) and *y*-axis (vertical) within the Cartesian coordinates are labeled. A development section ($\approx 55d$) is set preceding, followed by the heating region of $300d$. The central angle $\theta = 0^\circ$ denotes the top peak, with $\theta = 180^\circ$ representing the bottom peak. To implement uniform sand-grain wall roughness, roughness height (K_s) and a fixed roughness constant ($C_s = 0.5$: appropriate for uniform sand-grains) are set. A mesh with a grid number of approximately 3.5×10^6 was established, and the refinement was made with inserted inflation layers near the wall to guarantee $y^+ < 1.0$. The boundary assignment and calculation strategies can be referred to in our previous work ([Wang et al., 2019](#)) on horizontal sCO₂ computations. For the grid independence examination, the grid number is increased by nearly doubling it, and the deviation of averaged wall temperatures computed using different grid densities is found to be less than 1.5%.

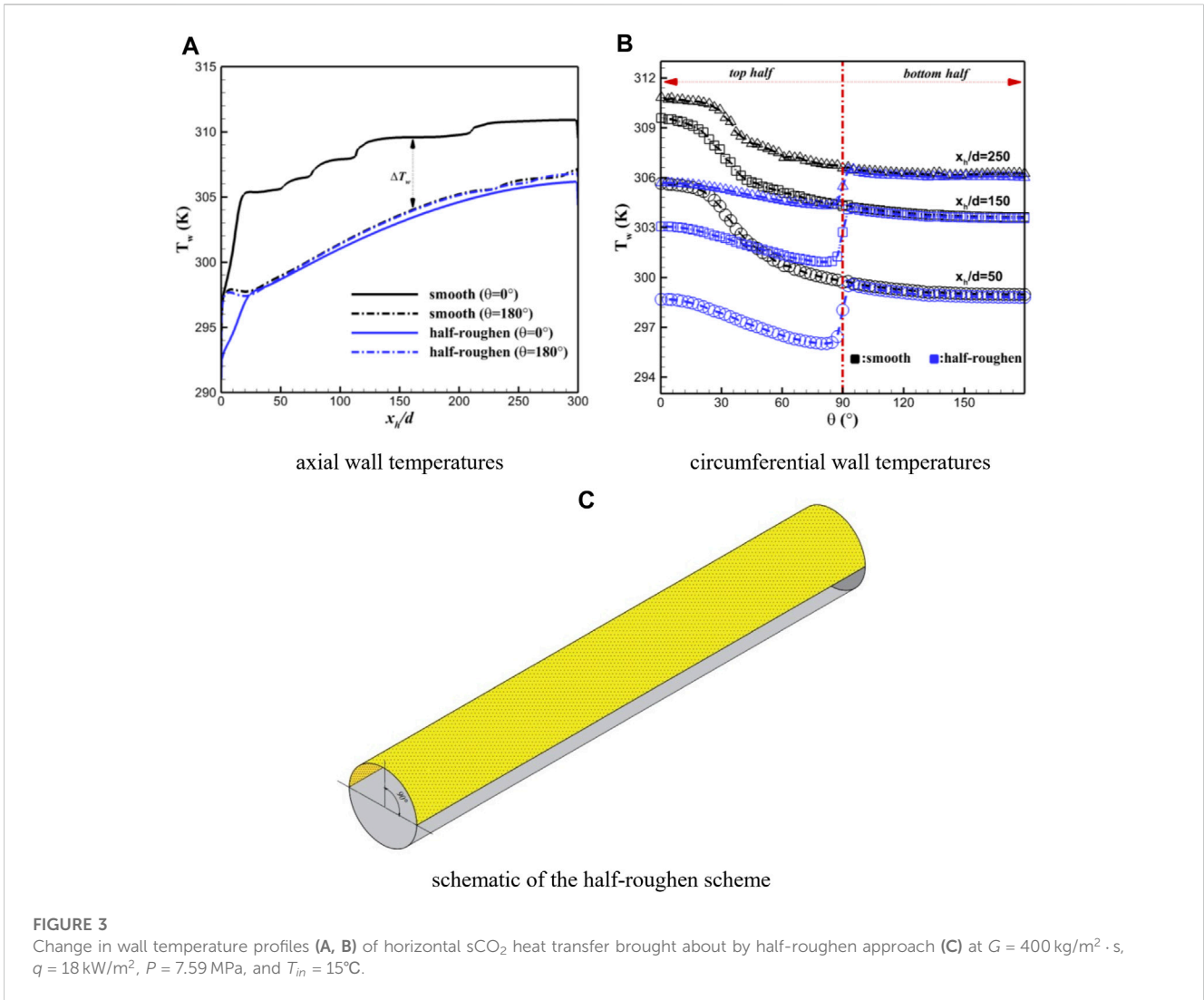


TABLE 2 Simulation conditions.

Case code	Mass flux G ($\text{kg/m}^2 \cdot \text{s}$)	Heat flux q (kW/m^2)	Pressure P (MPa)	Inlet temperature T_{in} ($^\circ\text{C}$)	Relative roughness height Δ
Baseline (BL)	400	18	7.59	15	0, 1/504, 1/252, 1/120, 1/60, 1/30
G300	300	18	7.59	15	
G500	500				
Q8	400	8	7.59	15	
Q28		28			
P8.5	400	18	8.5	15	
P9.5			9.5		
T20	400	18	7.59	20	
T25				25	

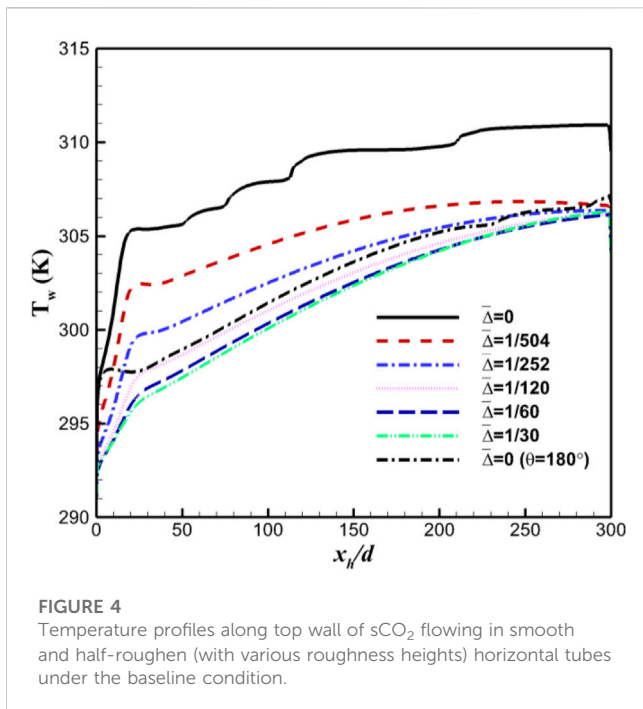


FIGURE 4
Temperature profiles along top wall of sCO₂ flowing in smooth and half-roughen (with various roughness heights) horizontal tubes under the baseline condition.

2.3 Model validations

The experiments conducted by [Chen et al. \(2022\)](#) are employed for the validation of the SST $k-\omega$ model on reproducing sCO₂ rough heat transfer, where the electrical discharge machining was utilized to generate sand-grain roughness onto the inner wall of a 4.57 mm-diameter horizontal pipe and the roughness was measured using a measuring instrument of TR100. The axial wall temperature distributions were obtained within a wide operating range, and five different test cases were selected with varying operating parameters and roughness heights. The details are provided in the [Table 1](#).

[Figure 2](#) compares the simulated wall temperatures against the experimental data. Good consistencies were exhibited for all the cases, and the maximum deviation is within 6°C. For cases T1&T2, with the roughness height rising from 1.5 μm of the smooth tube to 40 μm, the wall temperatures decreased, indicating the improved heat transfer, and this trend was also well captured by the model. The underestimation by the computations might be attributed to the fact that in the actual physical tests, there exist wall roughness units with larger heights than the measured average value, which can result in more intensified turbulent activities.

2.4 Half-roughen scheme

As shown in [Figure 3A](#) for the smooth horizontal sCO₂ flows, because of buoyancy effects, an obvious gap exists for the wall temperature profiles over the two peak surfaces; turbulent heat transfer impairs at the top and behaves normally around the bottom. The heat transfer difference can be also reflected by the T_w circumferential distributions in [Figure 3B](#), where the

temperature starts to rise from the wall center line ($\theta = 90^\circ \rightarrow 0^\circ$). To mitigate the degraded heat transfer in the whole top half and then to level the peripheral distribution of wall temperature, the approach to half-roughen the horizontal pipe was applied. As illustrated in [Figure 3C](#), the wall roughness is incorporated by particularly targeting the top half with higher T_w values. The axial and circumferential distributions of wall temperatures of the half-roughen horizontal pipe under the same condition were added in [Figures 3A, B](#), respectively. As seen, the top wall temperatures are significantly reduced to nearly overlap the bottom values, the degradation in the top is greatly improved, and the heat transfer becomes more homogenous.

3 Results and discussion

CFD calculations involving a range of roughness heights and operating parameters were performed to form a systematic study. The condition details are listed in [Table 2](#). According to the classic tests on the piping flows with sand-grain roughness by [Nikuradse \(1950\)](#), five different values for the relative roughness heights ($\bar{\Delta} = \Delta/d$: 1/504, 1/252, 1/120, 1/60, 1/30) are used, and “ $\bar{\Delta} = 0$ ” denotes the smooth tube.

3.1 Baseline case

This section discusses the results of the baseline case, where medium-level buoyancy effects are induced under the specific condition. Since this work introduces sand-grain wall roughness aiming to relieve the top heat transfer degradation and then ameliorate heat transfer homogeneity, the wall temperature gap that directly illustrates the circumferential uniformity is presented. In addition, under the studied conditions of constant heat flux, the exhibited wall temperatures are able to well reflect the variations of the local heat transfer coefficient or Nusselt number. [Figure 4](#) displays the axial distributions of top wall temperatures of horizontal sCO₂ flowing in the smooth and various half-roughen tubes, where the bottom T_w values of the smooth pipe are appended as a representative to exhibit the temperature difference (as well for the subsequent analysis). Circumferential T_w profiles are not presented here due to the quite similar trends to those exhibited in [Figure 3B](#). As can be seen from [Figure 4](#), with the pipe half-roughened, the top wall temperatures decrease, and with the rising roughness height, the thermal entrance effect propagates further downstream. In the range of $\bar{\Delta} < 1/120$, the rising roughness height leads to a more pronounced decrease in the top wall temperatures, while a further increase beyond that range only brings around a slight difference and is likely to cause higher friction loss.

[Figure 5](#) compares the thermofluid behavior of horizontal sCO₂ flowing in the smooth and half-roughen ($\bar{\Delta} = 1/120$) pipes. As shown, for the smooth case ($\bar{\Delta} = 0$), the hotter and lighter sCO₂ fluids accumulate around the top, where the boundary gets thicker, then the velocity gradient declines, and finally, the turbulence weakens. As the uniform wall roughness is added onto the top half, the accumulation is broken up and shrinks, and then, turbulent

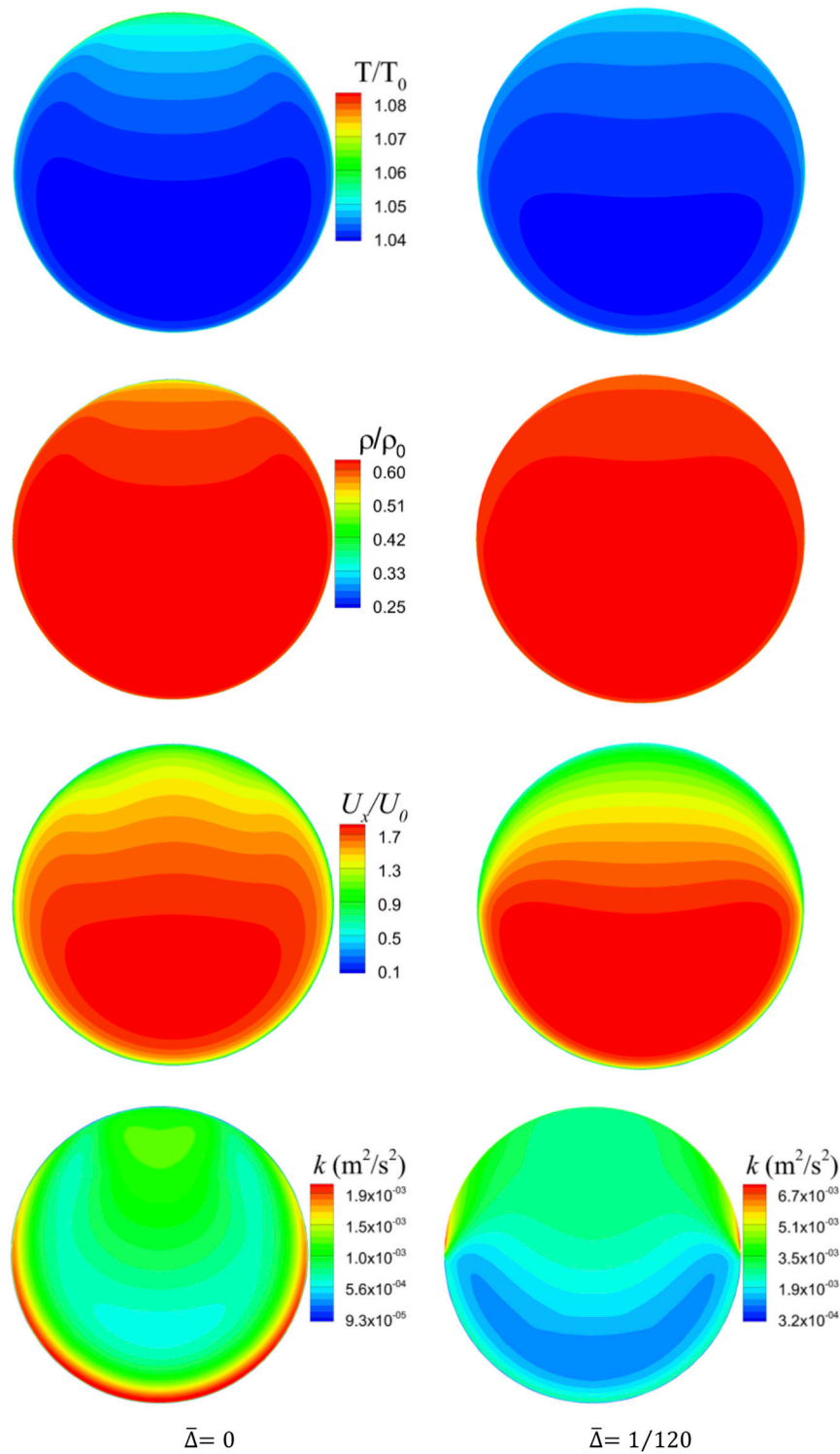
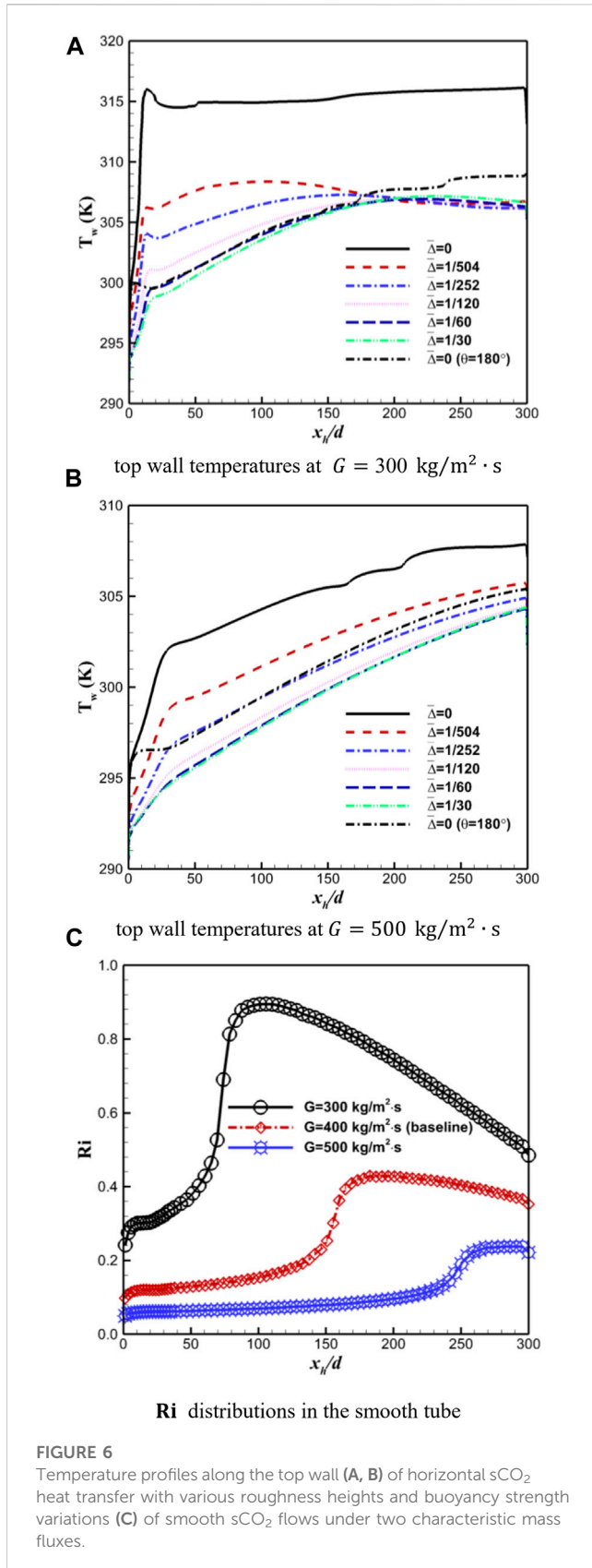


FIGURE 5 Influences of half-roughen wall roughness on thermofluids of horizontal sCO₂ flows, where temperature T , density ρ , and axial velocity U_x are normalized by inlet values.

activities near the wall intensify. For the turbulence kinetic energy distribution of the half-roughen tube, it can be noted that a peak appears near the wall center line where the roughness begins. This is

because when the buoyancy-induced secondary flow passes through the center point between the bottom and top halves, the abrupt change in the surface with roughness is likely to bring about strong



intensification of the turbulence, which can be also reflected by the sharply dropped wall temperatures of rough sCO₂ flows around $\theta = 90^\circ$, as displayed in Figure 3B.

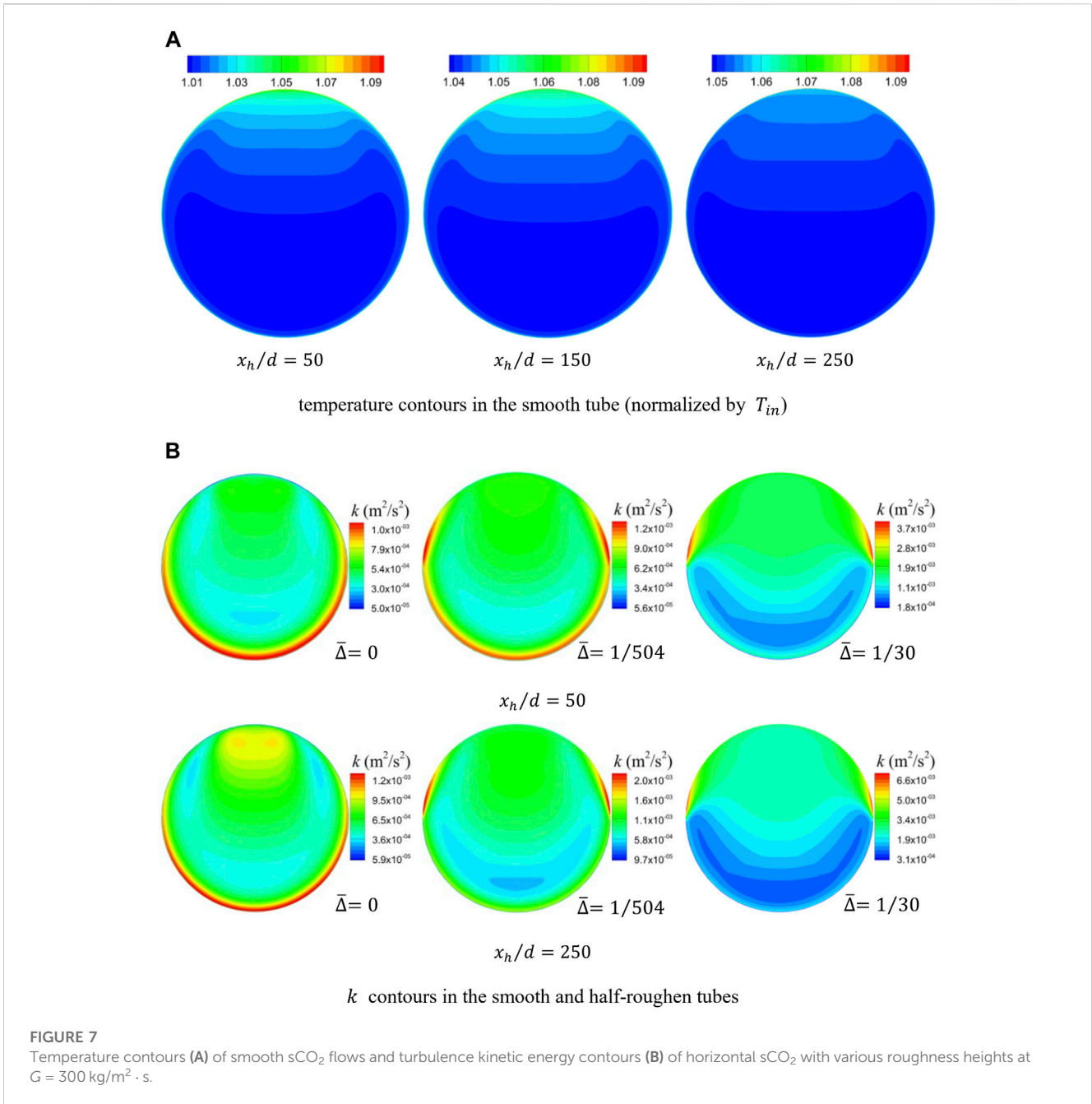
3.2 Simulations under different operating conditions

3.2.1 Effect of mass flux

The influences of various typical operating parameters are then analyzed. Figures 6A, B show the top wall temperature distributions under two different mass fluxes, where other parameters are maintained the same as the baseline case. As can be seen, when the value of mass flux decreases to $300 \text{ kg/m}^2 \cdot \text{s}$, the buoyant force increases and the T_w gap grows between the two peak surfaces, and the optimal roughness height to homogenize the circumferential distributions increases to $\bar{\Delta}_{opt} = 1/60$, which drops to $\bar{\Delta}_{opt} = 1/252$ for the increasing mass flux of $500 \text{ kg/m}^2 \cdot \text{s}$.

Comparing the two sets of distributions, it is worth noting that for the higher mass flux of $500 \text{ kg/m}^2 \cdot \text{s}$, the impact of roughness height ($\bar{\Delta} < 1/120$) is salient through the entire sCO₂ piping flows. However, the variations get complex under $G = 300 \text{ kg/m}^2 \cdot \text{s}$. In the upstream of horizontal sCO₂ flows within $x_h/d < 200$, the rising roughness height results in greater reduction in the top wall temperature, but the T_w values nearly remain unchanged with the varying roughness heights in the downstream at $x_h/d > 200$. The main reason behind these trends is that the buoyancy strength of sCO₂ flows is directly related with the q/G ratio and locally varies with the bulk stream as well.

Figure 6C presents the variations of Richardson number of smooth sCO₂ flows under the two mass fluxes, where the values of the baseline case are also added for comparison. This buoyancy parameter **Ri** ($\text{Ri} = \text{Gr}/\text{Re}^2$, $\text{Gr} = \rho_b(\rho_b - \rho_w)gd^3/\mu_b^2$) has been widely used in the literature (Chu and Laurien, 2016) for buoyancy quantification of heated horizontal sCO₂ fluid flows. As shown, when the mass flux declines with heat flux fixed, the q/G ratio rises, then the buoyancy strengthens, and the **Ri** values augment. According to the presented influences by the buoyancy on the thermohydraulic behaviors of horizontal sCO₂ fluids, the intensified buoyancy causes larger area of accumulation of low-momentum fluids in the top, thickening the boundary there that demands higher roughness height to totally break up. Considering the changing effect degree of roughness height along the bulk flow, the local **Ri** distributions under each case are discussed. As shown for the high-mass-flux flow ($G = 500 \text{ kg/m}^2 \cdot \text{s}$), the buoyancy strength slowly grows and maintains the relatively low level throughout the entire flow. However, under the low mass flux of $300 \text{ kg/m}^2 \cdot \text{s}$, the **Ri** value first rises to the peak ($x_h/d \approx 100$) and then drops in the downstream, which brings about the non-monotonic variation of boundary thickness at the top as well. Therefore, the roughness height exhibits the difference in the influence degree within the upstream and downstream. Based on the abovestated analysis, the converging point for the top wall temperature distributions of various roughness is expected to locate further downstream than the peak **Ri** position to meet the lower level of buoyancy strength and the thinner boundary of high-temperature sCO₂ flow, which has already been verified by the outcomes. Also, the impact of the roughness height gets suppressed in the far downstream under the baseline case, as seen in Figure 4. Figure 7A presents the temperature contours of horizontal sCO₂ flowing in smooth pipe at $G = 300 \text{ kg/m}^2 \cdot \text{s}$, where three different cross sections at $x_h/d = 50, 150$, and 250 are intercepted. It can be



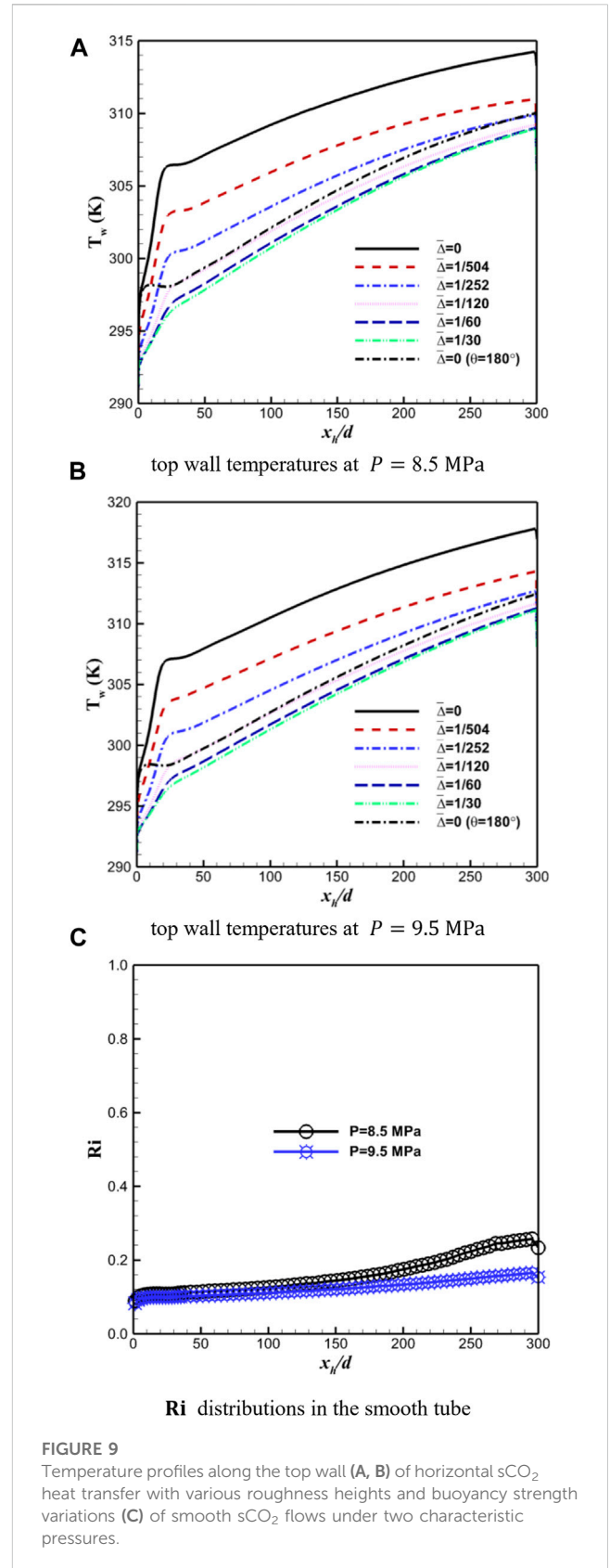
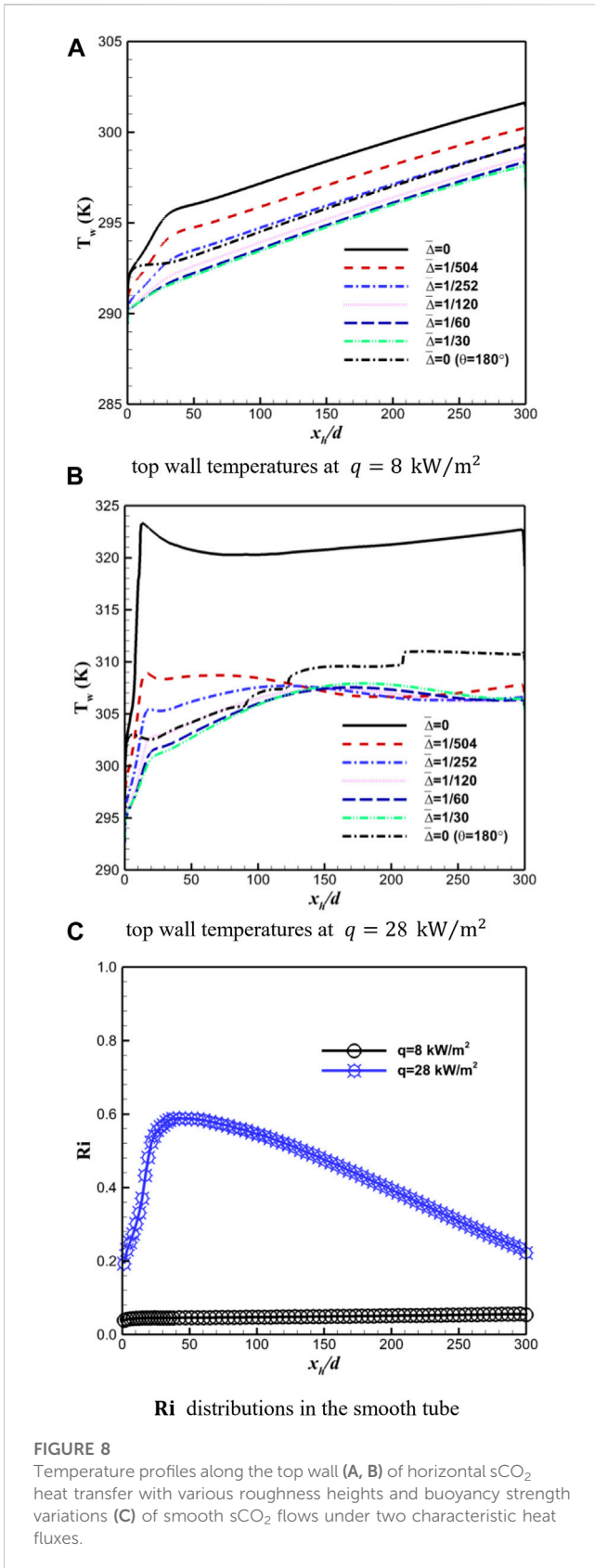
clearly observed that the high-temperature field of accumulation shrinks with the mainstream in the downstream.

The turbulence (k) distributions over the cross sections of horizontal sCO₂ flowing in the smooth and rough tubes at $G = 300 \text{ kg/m}^2 \cdot \text{s}$ are given in Figure 7B, in which the two typical cross sections within the far upstream ($x_h/d = 50$) and downstream ($x_h/d = 250$) are chosen and two extreme roughness heights are issued. As shown, the turbulent activities of smooth sCO₂ flows are more active near the bottom wall over both two profiles. When the roughness is incorporated, the differences in the turbulence kinetic energy distribution brought about by the roughness height are evident in the upstream region, where a large portion of the top wall is not effectively impacted by the low-height roughness and the k

values along the bottom wall are still much higher. However, within the downstream area, the introduced wall roughness with the lowest roughness height of $\bar{\Delta} = 1/504$ is able to effectively intensify the turbulence near the entire top wall to be even higher than those over the bottom.

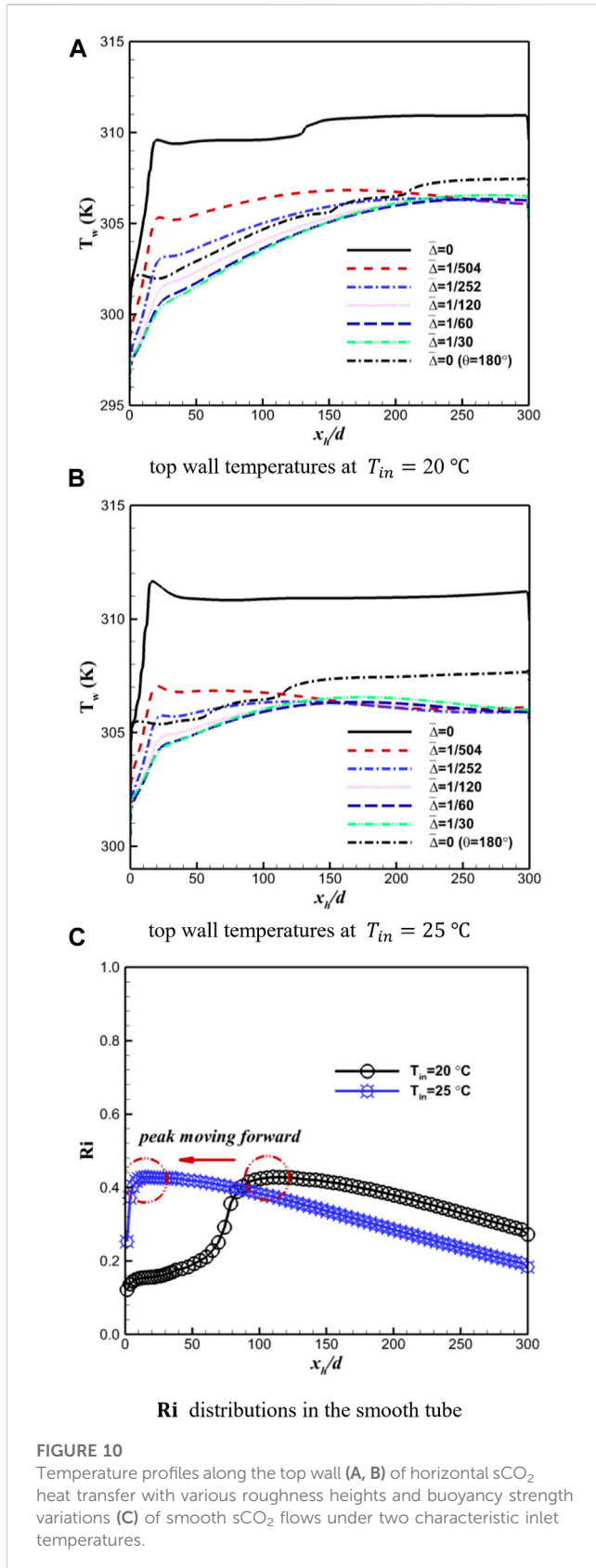
3.2.2 Effect of heat flux

With the change in the heat flux applied during the calculations, the calculation outcomes are displayed in Figure 8. For the low heat flux of $q = 8 \text{ kW/m}^2$, a roughness height of $\bar{\Delta} = 1/252$ is able to close the wall temperature gap well. As the q value increases up to 28 kW/m^2 , the temperature difference between the two peak walls remarkably grows, and similar to the trends exhibited in Figure 6A, the influence of the roughness height gets suppressed



around $x_h/d \approx 150$. According to the previous analysis on the buoyancy affecting the optimal roughness height, the variation in the heat flux also brings the changing q/G ratio, which directly

determines the level of buoyancy. As exhibited in Figure 8C, for buoyancy parameter distributions of smooth sCO_2 flows under these two heat fluxes, the Ri values are low and hardly vary with the



mainstream at $q = 8\text{ kW/m}^2$, whereas for the high heat flux of 28 kW/m^2 , with a peak value emerging in the very upstream, the non-monotonic trend is exhibited for the Ri distribution as well,

which causes the difference in the impact of varying roughness height between the upstream and downstream.

Here, it can be found that at $q = 28\text{ kW/m}^2$, although the T_w difference of smooth sCO₂ flows is more significant, the incorporated roughness (even with the low roughness height) is able to greatly decline the top wall temperature, as illustrated in Figure 8B. The response of T_w reduction to the roughness is more sensitive, which can be also reflected by the relatively larger temperature gap ($T_{w,bottom} > T_{w,top}$) in the downstream. This is because under high heat fluxes, the temperature gradient is higher in the near-wall sCO₂ fluids, where the thermal boundary is generally thinner. For this thin thermal boundary, the incorporated roughness, even with the low height, is expected to generate a big jump in the turbulent activities.

3.2.3 Effect of pressure

Figures 9A, B present the top wall temperature distribution with the different roughness heights under two larger operating pressures of 8.5 MPa and 9.5 MPa. It can be concluded that the optimum height nearly remains the same as the baseline case ($\bar{\Delta}_{opt} = 1/120$ in the upstream and $\bar{\Delta}_{opt} = 1/252$ in the far downstream), and the effect of rising operation pressure is slight. This can be explained by the fact that the pseudocritical temperature value increases with the increase in pressures, and the buoyancy strength maintains the low level within the regime of insignificant density variations, as shown in Figure 9C.

3.2.4 Effect of inlet temperature

With the inlet temperature increasing up to $T_{in} = 20^\circ\text{C}$ and 25°C , the outcomes are demonstrated in Figure 10. Compared to the baseline case, the optimum roughness height is still within the range of $1/252 - 1/120$, while the influence suppression of varying roughness heights is evident in the downstream of horizontal sCO₂ flows, and this happens earlier in the upstream at $T_{in} = 25^\circ\text{C}$. The trends can be explained by the distributions of local buoyancy parameter Ri of smooth sCO₂ flows shown in Figure 10C, where the non-monotonic variations are in presence for both flow cases and the peak value emerges earlier in the upstream under the higher inlet temperature of 25°C . This is because the larger inlet temperature approaches more the pseudocritical point where the dramatic density variations are about to induce the significant buoyancy effect. Regarding the suppressed influence of varying roughness heights in the downstream, combined with the distributions presented in Figure 6A and Figure 8B, it is interesting to find that the top wall temperatures usually converged to be around the pseudocritical point (305 K) at the studied pressure. This is because when the top wall temperature drops to be around the pseudocritical point, heat transfer reinforcement caused by the favorable thermophysical properties (such as the high specific heat and thermal conductivity) rather than the changing roughness height is dominant. In particular, the molecular Prandtl number of sCO₂ also reaches its peak, leading to the reinforced heat transfer, and then, the thermal boundary becomes thinner and could be totally destroyed by the small roughness size.

TABLE 3 Overall buoyancy level and optimal roughness height of various horizontal sCO₂ flows.

Case code	Average buoyancy parameter Ri_{ave}	Optimal roughness height $\bar{\Delta}_{opt}$ (normalized by diameter)
BL	0.188	1/252–1/120
G300	0.925	1/60
G500	0.078	1/252
Q8	0.050	1/252
Q28	0.563	1/120
P8.5	0.144	1/252–1/120
P9.5	0.124	1/252–1/120
T20	0.441	1/252–1/120
T25	0.399	1/252–1/120

3.3 The overall evaluations

The buoyancy effect is critical in influencing the optimum roughness height of the half-roughen scheme to close the temperature gap between the two peak walls of horizontal sCO₂ flows. Table 3 computes the average buoyancy parameter Ri_{ave} of smooth sCO₂ flows under all the nine operating conditions investigated in this work, where the optimal (relative) heights of wall roughness to obtain heat transfer uniformity are listed, correspondingly. For the calculation of Ri_{ave} to demonstrate the overall buoyancy strength, the circumferentially averaged wall temperature and arithmetic mean bulk temperature are used. It can be noted that as the overall buoyancy level grows, the optimal roughness height nearly monotonously augments.

4 Conclusion

Accounting for the particular sCO₂ heat transfer features within the horizontal orientations, the circular wall was half-roughened with sand-grain wall roughness to close the significant wall temperature gap over the perimeter. With the help of the validated SST $k-\omega$ model, numerous simulations were performed, and influences of the critical roughness height under a variety of operating conditions are discussed and analyzed in detail. The following conclusions can be drawn:

- Involving extensive operating conditions, horizontal sCO₂ heat transfer with sand-grain wall roughness can be well reproduced by the SST $k-\omega$ model, and the maximum deviation is within 6°C for wall temperature predictions.
- The wall temperature gap encountered in horizontal sCO₂ heat transfer can be effectively narrowed by the employed half-roughen scheme, and the circumferential homogeneity of heat transfer was greatly improved. An optimal roughness height exists, which increases with the rising q/G ratio while hardly changing with the rising pressure and inlet temperature.
- Buoyancy is a crucial factor that determines the influences of wall roughness and its optimal height. The intensified buoyancy recirculates more low-momentum fluids to be

accumulated in the top, which demands the larger roughness height to totally break. The local variations in the buoyancy strength lead to consequences as well. As the buoyancy level along the sCO₂ mainstream presents a non-monotonic distribution with a peak value emerging in the upstream, the influences of varying roughness heights will be greatly suppressed in the downstream, and the top wall temperatures are likely to be converged around the pseudocritical point.

Data availability statement

The original contributions presented in the study are included in the article/Supplementary material; further inquiries can be directed to the corresponding author.

Author contributions

JY: investigation, methodology, and writing—original draft. XX: visualization and software. GT: validation and software. JW: conceptualization, funding acquisition, methodology, investigation, validation, and writing—review and editing. All authors contributed to the article and approved the submitted version.

Funding

This work was financially supported by the National Natural Foundation of China (Project No. 52006248) and Shenzhen Science and Technology Program (Project No. RCBS20210706092408013).

Conflict of interest

The authors declare that the research was conducted in the absence of any commercial or financial relationships that could be construed as a potential conflict of interest.

Publisher's note

All claims expressed in this article are solely those of the authors and do not necessarily represent those of their affiliated

organizations, or those of the publisher, the editors, and the reviewers. Any product that may be evaluated in this article, or claim that may be made by its manufacturer, is not guaranteed or endorsed by the publisher.

References

- Chen, J., Yang, S-G., Zhao, R., and Cheng, W-L. (2022). Experimental study on the effect of wall roughness on heat transfer characteristics of supercritical carbon dioxide in vertical tubes. *Int. J. Heat Mass Transf.* 196, 123258. doi:10.1016/j.ijheatmasstransfer.2022.123258
- Chen, J., Zhao, R., Nian, Y-L., and Cheng, W-L. (2023). Numerical study on the effects of cylindrical roughness on heat transfer performance and entropy generation of supercritical carbon dioxide in vertical tubes. *Int. J. Heat Mass Transf.* 208, 124060. doi:10.1016/j.ijheatmasstransfer.2023.124060
- Chu, X., and Laurien, E. (2016). Flow stratification of supercritical Co₂ in a heated horizontal pipe. *J. Supercrit. Fluids* 116, 172–189. doi:10.1016/j.supflu.2016.05.003
- Forooghi, P., Stripf, M., and Frohnappel, B. (2018). A systematic study of turbulent heat transfer over rough walls. *Int. J. Heat Mass Transf.* 127, 1157–1168. doi:10.1016/j.ijheatmasstransfer.2018.08.013
- Han, Z., Guo, J., Liao, H., Zhang, Z., and Huai, X. (2022). Numerical investigation on the thermal-hydraulic performance of supercritical Co₂ in a modified airfoil fins heat exchanger. *J. Supercrit. Fluids* 187, 105643. doi:10.1016/j.supflu.2022.105643
- Kumar, N., and Basu, D. N. (2021). Role of buoyancy on the thermalhydraulic behavior of supercritical carbon dioxide flow through horizontal heated minichannel. *Int. J. Therm. Sci.* 168, 107051. doi:10.1016/j.ijthermalsci.2021.107051
- Latini, B., Fiore, M., and Nasuti, F. (2022). Modeling liquid rocket engine coolant flow and heat transfer in high roughness channels. *Aerosp. Sci. Technol.* 126, 107672. doi:10.1016/j.ast.2022.107672
- Liu, Z. B., He, Y. L., Qu, Z. G., and Tao, W. Q. (2015). Experimental study of heat transfer and pressure drop of supercritical Co₂ cooled in metal foam tubes. *Int. J. Heat Mass Transf.* 85, 679–693. doi:10.1016/j.ijheatmasstransfer.2015.02.013
- Mao, S., Zhou, T., Wei, D., Liu, W., and Xue, C. (2022). Numerical investigation on flow and thermal performance of supercritical Co₂ in a horizontal ribbed tube. *J. Supercrit. Fluids* 187, 105644. doi:10.1016/j.supflu.2022.105644
- Mendez Cruz, C. M., and Rochau, G. E. (2018). *Sco₂ brayton cycle: Roadmap to Sco₂ power cycles Ne commercial applications*. Albuquerque, NM United States: Sandia National Lab. SNL-NM.
- Menter, F. R. (1994). Two-equation eddy-viscosity turbulence models for engineering applications. *AIAA J.* 32 (8), 1598–1605. doi:10.2514/3.12149
- Nikuradse, J. (1950). Laws of flow in rough pipes. *J. Appl. Phys.*, 3.
- Stimpson, C. K., Snyder, J. C., Thole, K. A., and Mongillo, D. (2016). Roughness effects on flow and heat transfer for additively manufactured channels. *J. Turbomach.* 138 (5), 051008. doi:10.1115/1.4032167
- Theologou, K., Mertz, R., Laurien, E., and Starflinger, J. (2022). Experimental investigations on heat transfer of Co₂ under supercritical pressure in heated horizontal pipes. *Energy* 254, 124171. doi:10.1016/j.energy.2022.124171
- Wang, J., Guan, Z., Gurgenci, H., Veeraragavan, A., Kang, X., and Hooman, K. (2019). A computationally derived heat transfer correlation for in-tube cooling turbulent supercritical Co₂. *Int. J. Therm. Sci.* 138, 190–205. doi:10.1016/j.ijthermalsci.2018.12.045
- Wu, P., Ma, Y., Gao, C., Liu, W., Shan, J., Huang, Y., et al. (2020). A review of research and development of supercritical carbon dioxide brayton cycle Technology in nuclear engineering applications. *Nucl. Eng. Des.* 368, 110767. doi:10.1016/j.nucengdes.2020.110767
- Yalcinkaya, R., and Biyikoğlu, A. (2012). On usage of super-critical carbon-dioxide in a geothermal power cycle. *J. Fac. Eng. Archit. Gazi Univ.* 27 (3).
- Yang, J., Yang, Z., and Duan, Y. (2021). Novel design optimization of concentrated solar power plant with S-Co₂ brayton cycle based on annual off-design performance. *Appl. Therm. Eng.* 192, 116924. doi:10.1016/j.applthermaleng.2021.116924
- Zhang, S., Xu, X., Liu, C., and Dang, C. (2020). A review on application and heat transfer enhancement of supercritical Co₂ in low-grade heat conversion. *Appl. Energy* 269, 114962. doi:10.1016/j.apenergy.2020.114962